Fiber optic system for in vivo real-time determination of tissue optical properties from steady-state diffuse reflectance measurements

Dam, J. S; Pedersen, C. B; Fabricius, P. E; Andersson-Engels, Stefan

Published in:
PHOTON MIGRATION, DIFFUSE SPECTROSCOPY AND OPTICAL COHERENCE TOMOGRAPHY: IMAGING AND FUNCTIONAL ASSESSMENT

DOI:
10.1117/12.407615

2000

Fiber optic system for *in vivo* real-time determination of tissue optical properties from steady-state diffuse reflectance measurements

Jan S. Dam[a,b], Carsten B. Pedersen[a], Paul Erik Fabricius[a], and Stefan Andersson-Engels[b].

[a] Bang & Olufsen Medicom a/s, DK-7600, Struer, Denmark.
[b] Lund Institute of Technology, P.O. Box 118, SE-22100, Lund, Sweden.

ABSTRACT

We present a versatile and compact fiber optic probe for real-time determination of the absorption and the reduced scattering coefficients from spatially resolved continuous wave diffuse reflectance measurements. The probe collects the diffuse reflectance at six distances in the range 0.6 - 7.8 mm at four arbitrary wavelengths, which were 660, 785, 805, and 974 nm in these experiments. The maximum sampling rate for one cycle of measurements including all four wavelengths is about 100 Hz. The absorption and the reduced scattering coefficients are extracted real-time from the probe measurements using multivariate calibration methods based on multiple polynomial regression and Newton-Raphson algorithms. The system was calibrated on a 6x7 matrix of Intralipid/ink phantoms with optical properties within typical biological ranges, e.g. at 785 nm, the ranges of the absorption and the reduced scattering coefficients, were 0 - 0.3 /cm and 6 - 16 /cm, respectively. Cross-validation tests shoved that the mean prediction error, relative to the ranges of absorption and the reduced scattering coefficients were 2.8 % and 1.3 %, respectively.

Keywords: Fiber Probe, Spatially Resolved, Diffuse Reflectance, Multivariate Calibration, Tissue Optical Properties

1. INTRODUCTION

The optical properties of human tissue, i.e. the absorption coefficient μ_a, the scattering coefficient μ_s, and the anisotropy factor g may provide important information on the composition and the physiological dynamics of the tissue. While μ_a may provide information on tissue chromophores, μ_s and g may be used to characterize the form, size, and concentration of various scattering components in the tissue. Due to the non-invasive possibilities, determination of tissue optical properties based on diffuse reflectance measurements has a great potential in the fields of biomedical diagnostics and monitoring. Diffuse reflectance measurements may be roughly divided into time-resolved[1], frequency-domain[2], and spatially resolved continuous wave methods[3]. Time-resolved and frequency-domain methods are often considered to be more accurate than spatially resolved methods for determination of absolute μ_a and μ'_s values, however they usually also require more expensive and bulky technology, which may restrict some biomedical implementations of these methods. In this talk, we present a fiber optic system for in vivo real-time determination of tissue optical properties based on spatially resolved continuous wave diffuse reflectance measurements at multiple wavelengths.

The system consists of a probe head with a source fiber in the center surrounded by five bundled detector fibers, which have been unraveled and mounted in five equally spaced concentric rings. Each of the five detector fibers is terminated on separate silicon detectors. In addition, three silicon detectors and a temperature sensor are mounted directly on the probe head. Thus, the diffuse reflectance can be collected at six distances, i.e. 0.6, 1.2, 1.8, 2.4, 3.0, and 7.8 mm. The source fiber is split into four separate fibers connected to four replaceable diode lasers. The wavelengths of the current diode lasers are 660, 785, 805, and 974 nm. The data acquisition is controlled by a laptop PC connected to a DSP board. The maximum sampling frequency of the system is about 100 Hz, i.e. data from all six distances at all four wave wavelengths, may be collected and stored in about 10 ms.

Accurate closed form mathematical analytical expressions for the spatially resolved diffuse reflectance $R(r)$ is strongly limited by requirements to the range of optical properties and the specific geometry of the setup[4]. Therefore, numerical

Photon Migration, Diffuse Spectroscopy, and Optical Coherence Tomography: Imaging and Functional Assessment, Stefan Andersson-Engels, James G. Fujimoto, Editors, Proceedings of SPIE Vol. 4160 (2000)

models[5] and multivariate calibration techniques[6] have been used to solve the inverse problem of extracting the optical properties from $R(r)$ measurements. In our case, we have chosen to calibrate the system on a 6x7 matrix of Intralipid/ink phantoms each with a distinct set of μ_a and μ'_s values. The ranges of the optical properties of the phantoms were chosen to match typical human skin tissue properties. At e.g. 785 nm the range of μ_a is 0 - 0.3 cm^{-1} and the range μ'_s is 6 - 16 cm^{-1}. In theory, it is possible to extract μ_a and μ'_s using $R(r)$ measurements at only two detector distances. Thus, we used a multiple polynomial regression method[7] to create a calibration model of $R(r)$ as a function of μ_a and μ'_s at the first and sixth detector of the fiber probe system, i.e. at the distances r_1 = 0.6 mm and r_2 = 7.8 mm., respectively. Subsequently, we applied a Newton-Raphson algorithm to extract μ_a and μ'_s from the probe measurements.

In the following, we first present the principles of the applied calibration and prediction algorithms. Next, we give a description of the probe specifications. Finally, we present and discuss the results attained from simulated numerical tests and phantom measurements.

2. GEOMETRY CONSIDERATIONS

The experimental results we present in this paper are based on a matrix of phantoms with 6x7 combinations of fixed Intralipid and ink concentrations. In order to investigate and determine the optimal probe geometry, we started out with generating a set of Monte Carlo simulations[8] with optical properties matching the phantom optical properties at 785 nm. Figure 1 shows the $R(r)$ profiles from these simulations.

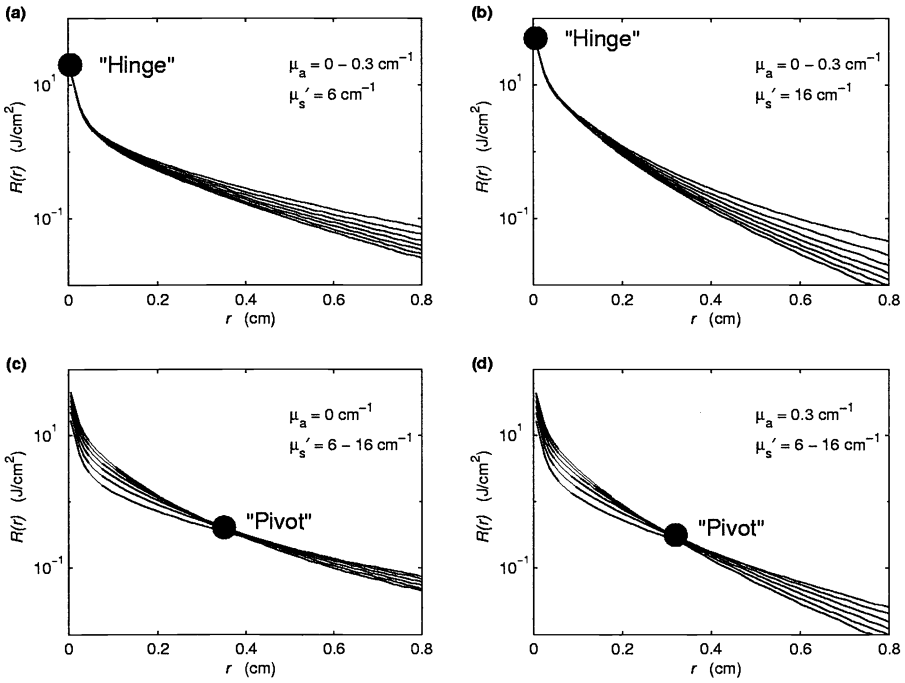

Figure 1. Monte Carlo simulated $R(r)$ data for various combinations of μ_a and μ'_s within ranges typical for skin tissue in the visible and near-infrared region. In panel (a) and (b), μ'_s is kept constant at 6 cm^{-1} and 16 cm^{-1}, respectively while μ_a is varied within the range 0 – 0.3 cm^{-1}. In panel (c) and (d), μ_a is kept constant at 0 cm^{-1} and 0.3 cm^{-1}, respectively while μ'_s is varied within the range 6 – 16 cm^{-1}. The *Hinge* and *Pivot* points indicates regions of r where $R(r)$ only changes slightly as a function μ_a and μ'_s, respectively.

In Figure 1(a) and (b) μ'_s is kept constant at values of 6 cm^{-1} and 16 cm^{-1}, respectively, while μ_a is varied. In these two cases, it appears that changes in μ_a only have a negligible effect on $R(r)$ at distances close to the source, i.e. the *hinge*

points in Figure 1(a) and (b). In Figure 1(c) and (d), μ_a is kept constant at values of 0 cm^{-1} and 0.3 cm^{-1}, respectively, while μ'_s is varied. Here, it is notable that there is very little variation in $R(r)$ at $r \approx 0.35$ cm, i.e. the *pivot points* in Figure 1(c) and (d). The $R(r)$ simulations in Figure 1(a) and (b) indicate that μ'_s may be determined with good accuracy from small source/detector distances solely. To determine μ_a also, Figure 1(c) and (d) suggest that $R(r)$ measurements close to the pivot point should be included, since there is little variation in $R(r)$ as a function of μ'_s at this distance. Although, other authors[9,10] also support this argumentation, we have based our experiments in this paper on close range distances in conjunctions with distances well beyond the pivot point. We did this, because our previous studies[6] showed that this geometrical configuration provided a better accuracy than a configuration with close range distances in conjunction with distances near the pivot point.

3. MULTIVARIATE CALIBRATION AND PREDICTION

In theory, μ_a and μ'_s may be determined using $R(r)$ data from only two of the six detector distances of the fiber probe. Figure 2 shows two surface plots of $R(r)$ at $r_1 = 0.6$ mm and $r_2 = 7.8$ mm as a function of μ_a and μ'_s. The plots are based on the 6x7 Monte Carlo simulated matrix we applied in the previous section. From Figure 1 it appears that r_1 corresponds to the *hinge point*, while r_2 corresponds to a point well beyond the *pivot point*.

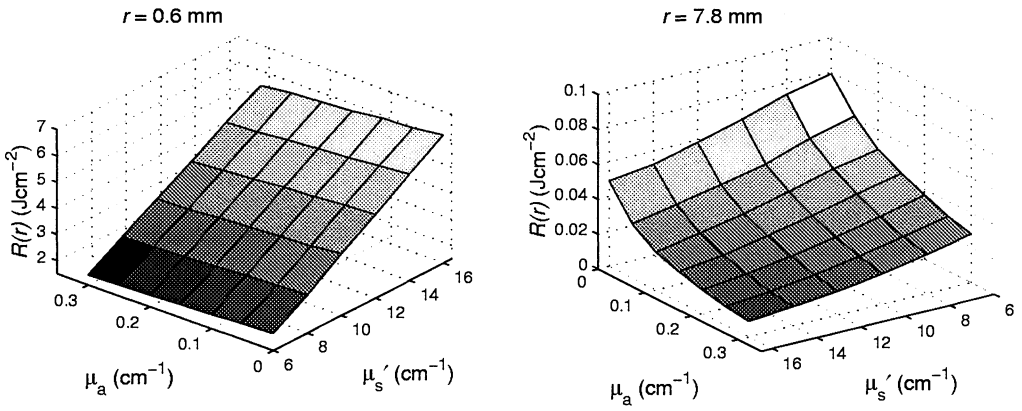

Figure 2. Surface plots of the 6x7 Monte Carlo simulated $R(r)$ matrix at $r_1 = 0.6$ mm and $r_2 = 7.8$ mm as a function of μ_a and μ'_s. Optical property units are in cm^{-1}.

The smooth and regular appearance of the two plots in Figure 2, indicates that $R(r, \mu_a, \mu'_s)$ at r_1 and r_2 may be fitted well by relatively simple functions. Building on our previous work[3], we thus applied multi polynomial regression (MPR) to create a calibration model of $R(r)$ as a function of μ_a and μ'_s at $r_1 = 0.6$ mm and $r_2 = 7.8$ mm. Then we subsequently used a Newton-Raphson algorithm to extract μ_a and μ'_s from real $R(r)$ measurements. The principles of the MPR method are as follows. We first determine $R(r)$ at r_1 and at r_2 for a set of calibration samples with well-defined optical properties and denote them $R_{1,cal}$ and $R_{2,cal}$. Then, we find a third order double-polynomial fit to $R_{1,cal}$ and $R_{2,cal}$:

$$R_{1,fit}(\mu_a, \mu'_s) = (a_0 + a_1\mu_a + a_2{\mu_a}^2 + a_3{\mu_a}^3)(b_0 + b_1\mu'_s + b_2{\mu'_s}^2 + b_3{\mu'_s}^3)$$
$$R_{2,fit}(\mu_a, \mu'_s) = (c_0 + c_1\mu_a + c_2{\mu_a}^2 + c_3{\mu_a}^3)(d_0 + d_1\mu'_s + d_2{\mu'_s}^2 + d_w{\mu'_s}^3) \quad (1).$$

Where, the a, b, c, and d 's are fitting coefficients determined by least-squares regression. $R_{1,fit}$ and $R_{2,fit}$ thus constitute the calibration model.

The next step is to solve the inverse problem of determining μ_a and μ'_s from $R(r)$ measurements on a set of prediction samples, i.e. $R_{1,meas}$ and $R_{2,meas}$. First we define:

$$F(\mu_a, \mu'_s) = R_{1,fit} - R_{1,meas}$$
$$G(\mu_a, \mu'_s) = R_{2,fit} - R_{2,meas} \qquad (2).$$

Then, we use a Newton-Raphson algorithm to perform converging iterative calculations of μ_a and μ'_s:

$$\left.\begin{aligned} -\begin{bmatrix} F(\mu_{a,k}, \mu'_{s,k}) \\ G(\mu_{a,k}, \mu'_{s,k}) \end{bmatrix} &= \begin{bmatrix} \frac{\partial F}{\partial \mu_a} & \frac{\partial F}{\partial \mu'_s} \\ \frac{\partial G}{\partial \mu_a} & \frac{\partial G}{\partial \mu'_s} \end{bmatrix} \begin{pmatrix} h_{a,k} \\ h_{s,k} \end{pmatrix} \\ \begin{pmatrix} \mu_{a,k+1} \\ \mu'_{s,k+1} \end{pmatrix} &= \begin{pmatrix} \mu_{a,k} \\ \mu'_{s,k} \end{pmatrix} + \begin{pmatrix} h_{a,k} \\ h_{s,k} \end{pmatrix} \end{aligned}\right\} \quad k = 0,1,2,3,\ldots, \qquad (3).$$

Where, h_a and h_s are correction terms of μ_a and μ'_s. The calculations continue until h_a and h_s have dropped below predefined maximum values.

The above prediction algorithms were implemented in Matlab and run on a 166 MHz PC. With this configuration, the prediction of a single set of μ_a and μ'_s could be performed in about 60 ms.

4. THE FIBER PROBE SYSTEM

Figure 3 shows the basics of the fiber probe system we have used to obtain the experimental results in this paper. The system consists of a probe head with a 200 µm source fiber in the center surrounded by five equally spaced concentric rings of 250 µm detector fibers. We chose this ring geometry instead of e.g. a simpler linear geometric configuration, partly to be able to collect more light at the farther distances, and partly to minimize any problems arising from tissue inhomogeneities during clinical measurements. The fibers of each single ring detector are bundled and terminated on separate silicon photo diodes. In addition, three photo diodes and a temperature sensor are mounted directly near the perimeter of the probe head. Thus, $R(r)$ can be collected at six distances, i.e. $r =$ 0.6, 1.2, 1.8, 2.4, 3.0, and 7.8 mm, respectively. The gain of each reflectance detector has been calibrated in an integrating sphere setup to obtain equal outputs at constant input light intensities. The source fiber is coupled into four separate fibers each connected to four replaceable low-power diode lasers. The diode lasers are mounted on a heat sink with a constant temperature maintained by an external controller. Furthermore, a separate reference detector monitors the output of the source fiber at the probe head. The diode lasers may be selected arbitrarily in order suit different applications.

In this paper we have used diode lasers with the wavelengths 660, 785, 805, and 974 nm, which are well suited for applications involving hemodynamic monitoring. The data acquisition and storage is controlled by a laptop PC connected to a digital signal processing (DSP) board. In each $R(r)$ measurement the detector hardware collects data simultaneously in eight parallel channels from the probe head, i.e. (a) from the six detector rings, (b) from the reference detector at the source fiber, and (c) from the temperature sensor. One cycle of four successive measurements (i.e. one at each wavelength) including dark measurements may be performed in about 10 ms, thus the maximum sampling rate of the system is about 100 Hz. To minimize any interference from background light or drift of the light sources, the dark measurements are subtracted from the measured reflectance data after which they are normalized relative to the source reference. The DSP board accomplishes this prior to the data are analyzed, displayed and stored by the PC.

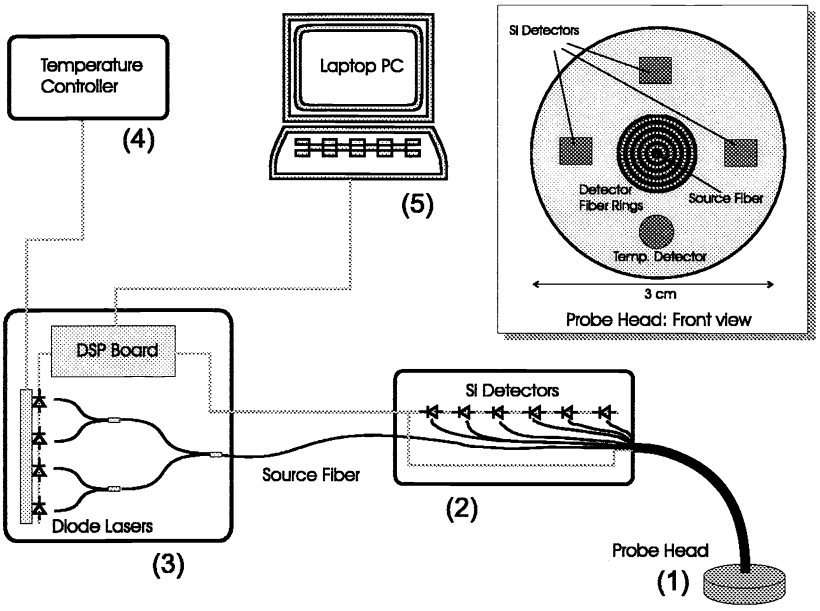

Figure 3. Diagram of the applied fiber optic system for $R(r)$ measurements. (1) Probe head with source and detector optical fibers mounted in a rotational symmetric configuration. (2) Handheld box with silicon photo diodes and amplifier electronics. (3) Stationary box containing a DSP board and the light sources, i.e. diode lasers. (4) External temperature controller to maintain a constant temperature of the diode lasers. (5) Laptop PC to analyze, display, and store the acquired $R(r)$ data.

5. RESULTS AND DISCUSSION

The prediction accuracy of the MPR method and the probe system was tested using leave-one-out cross validation of a 6x7 $R(r)$ data matrix. This means that we successively performed predictions using one set of $R(r)$ data for prediction and the data from the remaining 41 set of the 6x7 matrix for calibration. In order to insure that the calibration models covered all $R(r)$ variations, we only carried out predictions on the 4x5 interior subset of the 6x7 matrix. Figure 4 shows the prediction errors from cross validation prediction tests based on data from phantom measurements with the fiber probe and Monte Carlo simulations, respectively.

Due to the unknown numerical apertures of the fiber probe light source and detectors, we chose to calibrate the probe system directly on a set of phantoms instead of using a Monte Carlo based calibration model. The phantoms consisted of well-defined aqueous solutions of Intralipid and black ink. We determined the μ_a and μ'_s spectra of the Intralipid and the black ink from integrating sphere measurements and traditional transmission spectroscopy measurements. On the basis of these spectra, we mixed a 6x7 matrix of phantoms with μ_a and μ'_s ranges matching the 6x7 matrix of simulated data. The applied range of Intralipid concentrations were 0.6, 0.8, ...1.6 %, and the range of the ink concentrations were 0.0, 0.2, ...1.2 %. It should be noted, that the absorption of pure ink is much higher than that of typical biological substances, thus the ink concentrations refers to a premixed basic ink/water solution with a biological relevant absorption level. During the prediction experiments we calibrated the probe system directly to the concentrations of the Intralipid and the ink in the phantoms, assuming that the absorption of pure Intralipid and the scattering of the ink both were negligible.

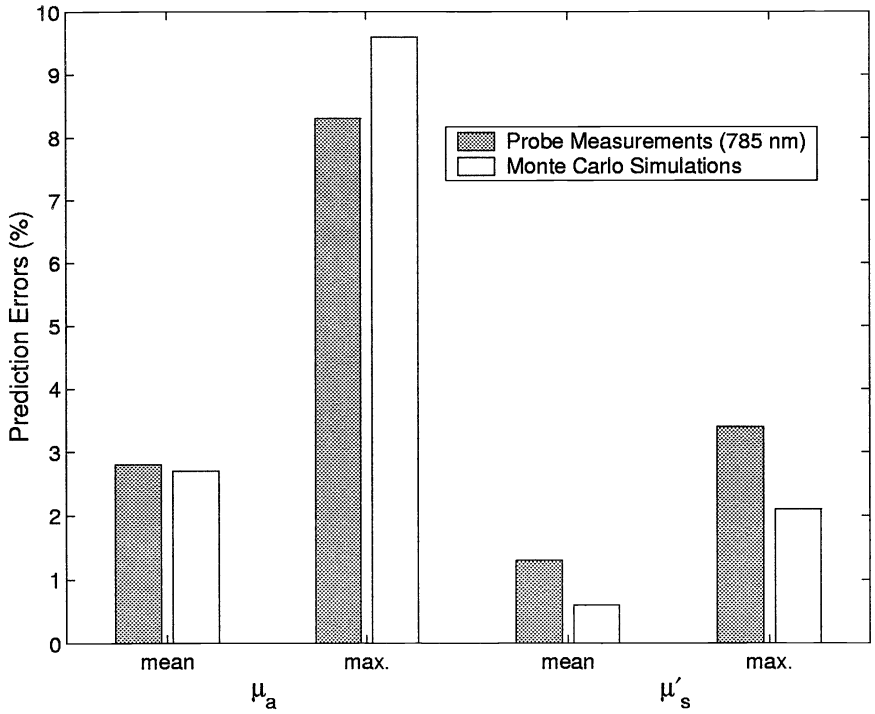

Figure 4. Mean and maximum prediction errors of μ_a and μ'_s from probe measurements and corresponding Monte Carlo simulations.

The prediction tests using Intralipid/ink phantoms showed a good accuracy comparable to the accuracy obtained on simulated data. Figure 4 only depicts the results from predictions at 785 nm. However, predictions at the three remaining wavelengths showed similar results, i.e. the mean prediction error at all four wavelengths is roughly 3 % for μ_a, and 1.5% for μ'_s. The prediction algorithm converged in all cases. In general, the prediction errors of μ_a are about twice as high as the errors of μ'_s. This may partly be attributed to the fact that μ_a is mainly determined on the basis of the $R(r)$ data at $r = 7.8$ mm, while μ'_s is almost solely determined from $R(r)$ data at $r = 0.6$ mm, where the signal level is about 1000 times the level at $r = 7.8$ mm. The μ_a predictions are therefore more sensitive to any background noise interference during the measurements.

From Figure 4 it appears that the maximum prediction errors of μ_a are relatively high (about 10%) for both the phantom measurements and the Monte Carlo simulations. However, numerical tests showed that this maximum error could be reduced to less than 4 % either by using a calibration model with a higher resolution (e.g. a 11x13 matrix) or by using all six source/detector distances instead of only two during calibration and prediction. In the latter case the six measured variables were reduced to two input variables using principal component analysis in order to comply with the Newton-Raphson algorithm. Both of these methods showed only a moderate effect on the mean prediction errors of μ_a and μ'_s.

6. CONCLUSIONS

We have presented a versatile, fast and accurate probe system and prediction technique for real-time non-invasive determination of tissue optical properties from spatially resolved continuous wave diffuse reflectance measurements.
The system and the technique provide a sound basis for future development of cost-effective and compact systems for non- or minimal-invasive medical diagnostics and monitoring. However, further work is required to explore the applicability for specific biomedical implementations.

ACKNOWLEDGEMENTS

The authors acknowledge the financial support from the Danish Academy of Technical Sciences

REFERENCES

1. Patterson M. S., Chance B., and Wilson B. C., "Time resolved reflectance and transmittance for the non-invasive measurement of tissue optical properties," Appl. Opt. 28, 2331-2336 (1989).

2. Chance B., Cope M., Gratton E., Ramanujam N., and Tromberg B., "Phase measurement of light absorption and scatter in human tissue," Rev. Scient. Instr. 69, 3457-3481 (1998).

3. Farrell T. J., Patterson M. S., and Wilson B., "A diffusion theory model of spatially resolved, steady-state diffuse reflectance for noninvasive determination of tissue optical properties *in vivo*," Med. Phys. 19, 879-888 (1992).

4. Wang L. V. and Jacques S. L., "Source of error in calculation of optical diffuse reflectance from turbid media using diffusion theory," Comp. Meth. Prog. Biomed. 61, 163-170 (2000).

5. Marquet P., Bevilacqua F., Depeursinge C., and De-Haller E. B., "Determination of reduced scattering and absorption coefficients by a single charge-coupled-device array measurement. I. Comparison between experiments and simulations," Opt. Eng. 34, 2055-2063 (1995).

6. Dam J. S., Andersen P. E., Dalgaard T., and Fabricius P. E., "Determination of tissue optical properties from diffuse reflectance profiles by multivariate calibration," Appl. Opt. 37, 772-778 (1998).

7. Dam J. S., Dalgaard T., Fabricius, P. E. and Andersson-Engels S., "Multiple polynomial regression method for determination of biomedical optical properties from integrating sphere measurements," Appl. Opt. 39, 1202-1209 (2000).

8. Wang L-H, Jacques, S.L. and Zheng L-Q, "MCML - Monte Carlo modeling of photon transport in multi-layered tissues," Compt. Meth. Prog. Biomed. 47, 131-146 (1995).

9. Mourant J. R., Bigio I. J., Jack D. A., Johnson T. M., and Miller H. D., "Measuring absorption coefficients in small volumes of highly scattering media: Source-detector separations for which path lenths do not depend on scattering properties," Appl. Opt. 36, 5655-5661 (1997).

10. Kumar G. and Schmitt J. M., "Optimal probe geometry for near-infrared spectroscopy of biological tissue," Appl. Opt. 36, 2286-2293 (1997).